Published in final edited form as:

J Mol Biol. 2020 June 26; 432(14): 4108–4126. doi:10.1016/j.jmb.2020.05.013.

Molecular mechanism of regulation of the purine salvage enzyme XPRT by the alarmones pppGpp, ppGpp, and pGpp

Brent W. Anderson[1,*], **Aili Hao**[1,*], **Kenneth A. Satyshur**[2], **James L. Keck**[2], **Jue D. Wang**[1]

[1]Department of Bacteriology, 1550 Linden Dr., Madison, WI, USA 53706

[2]Department of Biomolecular Chemistry, 440 Henry Mall, Madison, WI, USA 53706, University of Wisconsin-Madison

Abstract

The alarmones pppGpp and ppGpp mediate starvation response and maintain purine homeostasis to protect bacteria. In the bacterial phyla Firmicutes and Bacteroidetes, xanthine phosphoribosyltransferase (XPRT) is a purine salvage enzyme that produces the nucleotide XMP from PRPP and xanthine. Combining structural, biochemical, and genetic analyses, we show that pppGpp and ppGpp, as well as a third newly-identified alarmone pGpp, all directly interact with XPRT from the Gram-positive bacterium *Bacillus subtilis* and inhibit XPRT activity by competing with its substrate PRPP. Structural analysis reveals that ppGpp binds the PRPP binding motif within the XPRT active site. This motif is present in another (p)ppGpp target, the purine salvage enzyme HPRT, suggesting evolutionary conservation in different enzymes. However, XPRT oligomeric interaction is distinct from HPRT in that XPRT forms a symmetric dimer with two (p)ppGpp binding sites at the dimer interface. (p)ppGpp's interaction with an XPRT bridging loop across the interface results in XPRT cooperatively binding (p)ppGpp. Also, XPRT displays differential regulation by the alarmones as it is potently inhibited by both ppGpp and pGpp, but only modestly by pppGpp. Lastly, we demonstrate that the alarmones are necessary for protecting GTP homeostasis against excess environmental xanthine in *B. subtilis*, suggesting that regulation of XPRT is key for regulating the purine salvage pathway.

Correspondence: wang@bact.wisc.edu; Phone (608) 263-0307; Fax (608) 262-9865, 1550 Linden Dr., 6478 Microbial Sciences Building, Madison, WI 53706.

*These authors contributed equally

Brent W. Anderson: Validation, Formal analysis, Investigation, Writing-Original Draft, Writing-Review & Editing, Visualization
Aili Hao: Validation, Formal analysis, Investigation, Writing-Original Draft, Visualization
Kenneth A. Satyshur: Validation, Formal analysis, Investigation, Writing-Original Draft, Visualization
James L. Keck: Resources, Writing-Review & Editing, Supervision
Jue D. Wang: Conceptualization, Validation, Resources, Writing-Original Draft, Writing-Review & Editing, Supervision, Project administration, Funding acquisition

ACCESSION NUMBERS

Datasets used in this study: PDB ID: 1Y0B, PDB ID: 2FXV, PDB ID: 6D9S, PDB ID: 6D9R, GenBank accession no. CP020102 for *B. subtilis* NCIB 3610 genome. Coordinates and structure factors have been deposited in the Protein Data Bank with accession number 6W1I.

Declarations of interest: none

Keywords

phosphoribosyltransferase; oligomerization; PRPP; specificity; cooperativity

INTRODUCTION

The purine nucleotide GTP is a central molecule in DNA replication, RNA transcription, and protein translation. GTP can be synthesized either through an energetically costly *de novo* pathway or through efficient salvaging of preformed nucleobases. Nucleobases are found in environments such as in exudates secreted by plant roots where they can be scavenged by soil bacteria for efficient nucleotide synthesis [1,2]. The energetic benefit of the salvage reaction makes it the preferred pathway for GTP synthesis whenever nucleobases are available [3,4]. However, excess intracellular GTP can lead to deleterious effects [5], and how the salvage pathway is regulated to protect organisms against external nucleobase fluctuations remains incompletely understood.

In bacteria, purine salvage can be regulated through inhibition of a key salvage enzyme, HPRT, by the nucleotide alarmones ppGpp and pppGpp ((p)ppGpp) [5–10]. HPRT uses the essential metabolite phosphoribosyl pyrophosphate (PRPP) as a phosphoribosyl donor to convert the nucleobases guanine and hypoxanthine to GMP and IMP, respectively, which can then be converted to GTP (Fig. 1a). HPRT is inhibited by (p)ppGpp competing with PRPP for binding the enzyme active site, which maintains GTP homeostasis under high guanine influx conditions [10].

In the Gram-positive bacterium *Bacillus subtilis*, another phosphoribosyltransferase, XPRT, is also important for GTP synthesis. XPRT converts xanthine to XMP using PRPP as the phosphoribosyl donor (Fig. 1a) [11,12]. XPRT is part of the PRT protein family that uses nucleobase substrates but has evolutionarily diverged [13], as demonstrated by low sequence homology with HPRT (10% identical). XPRT is conserved in the bacterial phyla Firmicutes and Bacteroidetes and is found more limitedly in the phyla Actinobacteria, Deinococcus-Thermus, and Proteobacteria (Fig. 1b). XPRT is evolutionarily and structurally distinct from another phosphoribosyltransferase, XGPRT, that is found largely in Proteobacteria and has recently been identified as a (p)ppGpp target in *Escherichia coli* [8,9]. XPRT and XGPRT both convert xanthine to XMP, but the two enzymes are found with mutual exclusivity in bacterial species [12–14]. *B. subtilis* XPRT and *E. coli* XGPRT share only 12% amino acid identity, highlighting their evolutionary divergence. XPRT is a purine salvage enzyme conserved in many bacterial species, but how XPRT is regulated at an enzymatic level is poorly understood.

Here we reveal that XPRT from the firmicute *B. subtilis* is a regulatory target of (p)ppGpp as well as a target of the less well understood alarmone pGpp. Hereafter, we will refer to all three alarmones as (p)ppGpp unless otherwise noted. Similarly to HPRT, (p)ppGpp binds the XPRT active site using its PRPP binding motif to compete with substrate binding. However, the XPRT oligomeric interactions drastically differ from HPRT, resulting in unique regulatory features. First, (p)ppGpp binds an inter-subunit site comprised of residues from two monomers within an XPRT dimer, resulting in cooperative binding of the regulatory

ligand. Second, the XPRT binding pocket discriminates between pppGpp and ppGpp/pGpp through a flexible loop that covers the 5′-phosphate binding pocket, explaining why ppGpp and pGpp more strongly inhibit XPRT activity than pppGpp. Finally, (p)ppGpp is necessary for GTP homeostasis maintenance upon exposure to excess external xanthine in *B. subtilis*.

RESULTS

pppGpp, ppGpp, and pGpp bind and inhibit the activity of XPRT

We first examined whether *B. subtilis* XPRT is a binding target of (p)ppGpp. To do so, we used the differential radial capillary action of ligand assay (DRaCALA) [15] to quantify the interaction between XPRT and ^{32}P-labeled pppGpp and ppGpp. DRaCALA relies on the different migration properties of protein and ligand on nitrocellulose. Protein diffuses slowly but ligand diffuses rapidly when a solution is spotted on nitrocellulose. However, radiolabeled ligand interacting with protein co-migrates with the protein (e.g., Fig. 2a). This interaction can be quantified as the fraction of total ligand bound with the protein. Using DRaCALA to obtain binding curves between XPRT and ^{32}P-pppGpp and ^{32}P-ppGpp, we found that *B. subtilis* XPRT is a binding target of pppGpp (K_d = 9.6 μM) and ppGpp (K_d = 0.95 μM) (Fig. 2b). A third alarmone, pGpp, has been shown to be produced *in vitro* and has been detected *in vivo* in *B. subtilis* [16,17]. We found that XPRT also binds pGpp (K_d = 0.76 μM) (Fig. 2b). All three ligands interacted cooperatively with XPRT with Hill coefficients ≈ 2 for pGpp and ppGpp and ≈ 1.3 for pppGpp (Table 1).

To understand how these alarmones regulate XPRT, we tested their effect on XPRT activity. To measure XPRT activity, we used UV absorption (A_{252}) to detect XMP production from the substrates xanthine and PRPP (e.g., Fig. 2c), and initial velocities were calculated from the rate of changes in A_{252} absorption. We found that pppGpp, ppGpp, and pGpp all inhibited XPRT activity (Fig. 2c, 2d, and 2e). ppGpp and pGpp potently inhibited activity with IC_{50} values of 3.3 ± 0.1 μM and 0.96 ± 0.04 μM, respectively (Fig. 2d and 2e and Table 1, ± SEM). pppGpp was a weaker inhibitor with an IC_{50} value of 56.4 ± 1.8 μM. The weaker inhibition by pppGpp corresponds with its reduced affinity for XPRT compared to ppGpp/pGpp (Fig. 2b). This suggests that while all three alarmones regulate XPRT, it is differentially regulated by pppGpp and ppGpp/pGpp. Notably, the cooperativity we observed in alarmone binding (Fig. 2b) was also observed in the inhibition curves, which fit with apparent Hill coefficients ≈ 1.5 for pppGpp, 1.7 for ppGpp, and 1.6 for pGpp (Table 1).

(p)ppGpp binds the conserved XPRT active site, and a flexible loop covering the pocket differentiates between pppGpp and ppGpp/pGpp

Next, we structurally examined the molecular mechanism of the (p)ppGpp-XPRT interaction. A structure of *B. subtilis* XPRT bound to ppGpp had already been deposited in the Protein Data Bank (PDB ID **1Y0B**) by the Midwest Center for Structural Genomics, although the 5′-phosphates of ppGpp were not modeled in the deposited structure. Using the unmodeled F_o-F_c difference density, we showed that there is sufficient density for a 5′-diphosphate in the ligand's binding pocket (Fig. 3a). Further refinement with ppGpp strongly supported the presence of a ppGpp molecule in the pocket (Fig. 3b). The final structure is at 1.8 Å resolution with R_{work}/R_{free} values of 0.160/0.208 (Table 2). XPRT-

ppGpp crystallized as a tetramer in the asymmetric unit, but PISA analysis (Protein interfaces, surfaces, and assemblies' service at European Bioinformatics Institute) predicts the biological unit to be a dimer (Fig. 3c) [18].

The XPRT active site comprises four loops (I, II, III, IV) (Fig. 3b). ppGpp binds this site in XPRT with its phosphates extending between loops I and III and the purine base positioned below loop IV (Figs. 3b and 4a). Most residues interacting with ppGpp are contained within one monomer (Fig. 4a). However, the second monomer in the XPRT dimer is also involved through a loop that extends over the ppGpp binding pocket (Fig. 4a). We define this loop as the "bridging loop" since it bridges the monomer-monomer interface.

The residues that interact with ppGpp include peptide backbone interactions of loops I and III that coordinate the 3′- and 5′-phosphates (Figs. 4a and S1). XPRT Phe126 also forms π-stacking interactions below the guanine ring of ppGpp, Leu85 from the bridging loop forms a hydrophobic hood above the guanine ring, and Lys156 coordinates the exocyclic oxygen from the base (Fig. 4a). XPRT Arg80, Lys81, Ser98, and Asn129 side chains all form hydrogen bonds with ppGpp's phosphates (Figs. 4a and S1).

To test whether these residues are indeed involved in their interaction with ppGpp *in vitro*, we created variants of Phe126, Asn129, and Lys156, and found that each variation resulted in a stably folded protein yet with weakened interactions with ^{32}P-ppGpp (Fig. 4b and 4c). We also created variants at Arg80, which interacts with ppGpp from the bridging loop (Fig. 4a). These variants interacted very weakly with ^{32}P-ppGpp, although the variants' protein stability was also compromised (Fig. 4b and 4c).

Since XPRT orthologs are conserved across Firmicutes and Bacteroidetes and are found in other bacterial phyla (Fig. 1b), we examined the conservation of the binding pocket across these phyla. We aligned 62 bacterial XPRTs and constructed a frequency logo of the (p)ppGpp-interacting residues (Fig. 4d). The binding pocket is strikingly conserved, with nine of the 16 residues being invariant (Glu58, Ser60, Lys81, Ser98, Asp124, Asp125, Phe126, Ala128, and Lys156). We conclude that the (p)ppGpp binding pocket is conserved across bacterial XPRTs.

The XPRT-ppGpp structure provides an explanation for our earlier observation that ppGpp or pGpp are stronger inhibitors of XPRT than pppGpp (Fig. 2c and 2d). In the structure, loop II forms a hood over the 5′-phosphate binding site (Fig. 4e), compressing the pocket where the 5′-phosphates of pppGpp, ppGpp, and pGpp are positioned. Fewer 5′-phosphates in pGpp and ppGpp likely allow the inhibitor to better bind the active site and potently inhibit enzyme activity.

In summary, pppGpp, ppGpp, and pGpp bind the conserved XPRT active site, and XPRT displays differential regulation by pppGpp and ppGpp/pGpp due to a loop conformation that compresses the 5′-phosphate binding site.

(p)ppGpp competes with PRPP to inhibit XPRT

We had previously obtained the co-structure of (p)ppGpp with the purine salvage enzyme HPRT [10]. Overlaying the structures of ppGpp-XPRT and ppGpp-HPRT [10] shows that

both ligands bind the enzymes' active sites in a similar conformation (Fig. 5a). We also overlaid the XPRT-ppGpp complex with HPRT bound to substrates PRPP and 9-deazaguanine (an inactive guanine analog) (Fig. 5b) [10]. Notably, ppGpp overlaps significantly with the substrates. The guanine ring of ppGpp likely binds in a position similarly to xanthine. The 5′-phosphates of ppGpp and PRPP share the same pocket, and the 3′-phosphates of ppGpp overlap with the 1′-phosphates of PRPP (Fig. 5b). XPRT variants with weakened (p)ppGpp interaction (Fig. 4b) also had compromised enzymatic activity (Fig. S2), supporting the structural model that (p)ppGpp and substrates share the same binding pocket.

Next, we examined whether (p)ppGpp competes with PRPP to inhibit XPRT using steady-state kinetics. We measured initial velocities of XPRT enzymatic reactions by examining the rate of synthesis of XMP at varied pppGpp and PRPP concentrations (Fig. 5c). The data best fit a global competitive inhibition model, demonstrating that (p)ppGpp competes with PRPP (Fig. 5c and 5d). In addition, the kinetic data yielded a K_i for pppGpp of 2.5 μM and a K_m for PRPP of 69 μM. Together with the structure, these data validate XPRT as a (p)ppGpp target and show that (p)ppGpp competes with PRPP for binding the active site to inhibit the enzyme.

(p)ppGpp stabilizes XPRT dimers by establishing electrostatic interactions bridging the monomer-monomer interface

XPRT is an unstable dimer with a reported tendency to dissociate to monomers [12]. Although the majority of (p)ppGpp binding residues are found within a single XPRT monomer, both monomers in an XPRT dimer are involved in binding each molecule of ppGpp (Figs. 4a and 6a). The second monomer contributes the bridging loop (residues 80–89) to the ppGpp binding site (Fig. 6b). Leu85 in this loop creates a hydrophobic hood for the guanine ring of ppGpp (Fig. 4a). The bridging loop also contains Arg80 and Lys81 (Fig. 6b). Lys81 contacts the 3′-phosphates of the ppGpp within its own monomer, while Arg80 reaches across the monomer-monomer interface to contact the 3′-phosphates of ppGpp in the adjoining monomer (Fig. 6b). In this way, (p)ppGpp creates a network of electrostatic interactions bridging the XPRT monomer-monomer interface.

The importance of the 3′-phosphates of (p)ppGpp for bridging the monomer-monomer interface is apparent when comparing structures of ppGpp-bound and GMP-bound XPRT [12]. GMP binds the active site similarly to ppGpp (Fig. 6c). However, since GMP lacks the 3′-phosphates of ppGpp, there is no interaction with the bridging loop and the loop is flipped away from the binding pocket (Fig. 6c). We tested the ability of GMP, GDP, and GTP to inhibit XPRT activity and found that all three nucleotides exhibit greatly reduced capacity to inhibit XPRT compared to their pGpp, ppGpp and pppGpp counterparts (Fig. 6d). These data suggest that the 3′-phosphates of (p)ppGpp are critical for binding and inhibiting XPRT.

Based on the structural evidence for the importance of the bridging loop and 3′-phosphate interaction, we propose a model to explain the cooperative (p)ppGpp binding we observed (Fig. 2): ppGpp binding to one site in an XPRT dimer would increase the affinity for ppGpp binding to the second site. This led us to predict that (p)ppGpp stabilizes the XPRT dimer by

providing additional interactions for holding the monomers together. With size exclusion chromatography, we found that apo XPRT eluted at a molecular weight between monomer and dimer as previously reported (Fig. 6e) [12]. While higher concentrations of XPRT favored the dimeric population, XPRT did not elute as a stable dimer. However, the addition of ppGpp in the mobile phase stabilized the dimeric XPRT population (Fig. 6e). These data support that (p)ppGpp can stabilize the interaction between two XPRT monomers. Overall, (p)ppGpp stabilizing XPRT dimers through interactions with the bridging loop provides a mechanism for cooperative inhibition of XPRT by (p)ppGpp.

(p)ppGpp protects against excess environmental xanthine

XPRT converts the purine base xanthine to the GTP precursor XMP. Xanthine is a nutrient that can be imported from the environment by xanthine permease. In *B. subtilis*, XPRT is encoded by *xpt*, located in the same operon as xanthine permease, and is transcriptionally regulated by a purine-sensing riboswitch (Fig. 7a) [11]. XPRT has been shown to be expressed at copy numbers of ~1,600–14,500 per cell across a variety of conditions, which allows the cell to effectively salvage xanthine [19–21].

Since *B. subtilis* is capable of salvaging xanthine for GTP synthesis, we sought to understand the importance of (p)ppGpp in regulating xanthine utilization. We added xanthine to wild type and (p)ppGpp-null ((p)ppGpp^0) *B. subtilis* growing exponentially in a defined glucose medium supplemented with the amino acids VILMTHRW to support the growth of (p)ppGpp^0. We then assessed GTP levels by thin layer chromatography. We found that GTP levels from xanthine-treated (p)ppGpp^0 *B. subtilis* were elevated relative to wild type (Fig. 7b). Higher GTP levels can promote growth, but too much GTP has been associated with reduced fitness of *B. subtilis* [5]. We next examined the effect of xanthine on *B. subtilis* fitness by measuring colony forming units before and several time points after xanthine addition. We found that in (p)ppGpp^0 *B. subtilis*, the addition of xanthine caused a significant reduction in viability (Fig. 7c). The reduced viability with xanthine can be attributed to XPRT since viability of a (p)ppGpp^0 *xpt* mutant is unaffected by xanthine (Fig. 7c). Altogether, these data reveal that excess environmental xanthine can disrupt GTP homeostasis and cell viability, and (p)ppGpp is necessary to protect GTP homeostasis.

DISCUSSION

(p)ppGpp is known to interact with multiple cellular targets, both at induced levels and basal levels, to protect cells against stress and maintain homeostasis. Here we combined structural and biochemical analyses to characterize a new (p)ppGpp target, the enzyme XPRT. We showed that (p)ppGpp binds to its active site at a PRPP binding motif and competes with substrate binding. We identified several unique features of regulation of XPRT due to its distinct oligomeric interactions, resulting in cooperativity and differential selectivity of alarmones. Our data indicate that basal levels pppGpp, ppGpp, and pGpp potently regulate XPRT activity to maintain GTP homeostasis even without nutrient deprivation. Combined with our previous results that (p)ppGpp inhibits the purine salvage enzyme HPRT [10], these data strengthen the model that basal (p)ppGpp protects GTP homeostasis against excess

environmental purines by gating all purine entry points through inhibition of salvage enzymes.

Regulation of XPRT by basal and induced levels of (p)ppGpp maintains purine homeostasis

(p)ppGpp protects bacteria at basal and starvation-induced levels, and our study suggests that both levels of the alarmones regulate XPRT. In *B. subtilis* and other firmicutes, induced (p)ppGpp reduces GTP levels during nutrient starvation to rewire the transcriptome for growth with limited nutrients [22,23]. In *B. subtilis*, pppGpp and ppGpp accumulate to mM levels during nutrient starvation, with pppGpp being approximately twice as abundant as ppGpp [5,24]. XPRT is inhibited by ppGpp and pppGpp with IC_{50} values ~ 3 μM and ~ 56 μM, respectively. This indicates that XPRT activity is potently inhibited during nutrient starvation. Along with GMK, HPRT, and IMPDH, XPRT is now another enzyme in the GTP synthesis pathway that can be controlled by (p)ppGpp during nutrient stress [5,6,24–26].

In addition to starvation-induced conditions, the regulation of XPRT by basal levels of (p)ppGpp is important for purine homeostasis. (p)ppGpp protects GTP homeostasis against excess external xanthine, suggesting that basal (p)ppGpp regulation of XPRT is important for regulating GTP levels. GTP is critical for growth and correlates with growth rate in *B. subtilis*, yet excess GTP is detrimental to viability [5,27]. By inhibiting XPRT activity at basal levels, (p)ppGpp can control the amount of xanthine salvaged for GTP synthesis throughout growth. Basal levels of pGpp and (p)ppGpp are below 30 μM in *B. subtilis* [5,17], and since pGpp and ppGpp are much stronger inhibitors than pppGpp, it is likely that pGpp and ppGpp contribute the most to basal regulation of XPRT.

An accumulation of GTP in (p)ppGpp^0 *B. subtilis* results in reduced viability during growth with environmental xanthine. We also observed this effect with excess environmental guanine and guanosine (Figure S3) [5]. Guanine causes a greater killing of (p)ppGpp^0 cells than we observed with xanthine, likely because guanine causes up to a 16-fold increase in (p)ppGpp^0 GTP levels whereas we observed ~6-fold increase in (p)ppGpp^0 GTP levels during growth with xanthine. The acute increase in GTP during growth with guanine likely makes guanine more toxic to (p)ppGpp^0 than xanthine. Xanthine may have less of an effect on GTP levels and viability of (p)ppGpp^0 since XPRT is weakly inhibited by GMP (Figure 6d), which would accumulate during growth with xanthine. Furthermore, while guanine is converted in a single reaction to GMP by HPRT, xanthine's conversion to GMP is dependent on both XPRT and GMP synthase, which catalyzes the conversion of XMP to GMP. The mechanism underlying the toxicity of high GTP remains an interesting outstanding question.

Environmental purine bases are a ready source of nucleotides for bacteria, but their utilization requires the uptake of purines by membrane-bound permeases followed by their conversion to nucleotides by phosphoribosyltransferases (PRTs). Permeases and PRTs function closely in the same metabolic pathway, and in the case of XPRT and the xanthine permease PbuX in *B. subtilis*, they can be genetically linked in the same operon (Fig. 7a) [11]. In fact, the phosphoribosylation system for purine bases is so closely linked that PRTs were initially reported to be membrane-bound enzymes that performed both uptake and phosphoribosylation [6,28]. Intriguingly, the isolation of HPRT in membrane vesicles and

reported membrane-association of human HPRT1 suggests that PRTs may function in physical proximity with the permeases providing their substrates [6,29]. It has also been suggested that PRT-catalyzed conversion of purine base to nucleotide could drive the uptake of purine bases via group translocation [30]. Given the metabolic and possible physical proximity between PRTs and permeases, (p)ppGpp inhibition of PRTs like XPRT and HPRT seems to control both the uptake and conversion of purine bases to nucleotides.

Structural insight into purine base discrimination by XPRT

(p)ppGpp binds XPRT similarly to substrates even though XPRT strictly uses xanthine and not guanine as a substrate [12]. How is XPRT able to recognize both xanthine and the guanine ring of (p)ppGpp? Xanthine and guanine are highly similar. For example, both xanthine and guanine have a hydroxyl group at the C6 position that interacts with the side chain of XPRT Lys156. The one difference between xanthine and guanine is at the C2 position of the purine ring, where xanthine has a hydroxyl group and guanine has an amino group. Importantly, the residue that interacts with this moiety, Asn27, can form a hydrogen bond with both groups. It can be a proton acceptor when interacting with guanine, and upon rotation of the side chain, it can be a proton donor when interacting with xanthine [12]. XPRT uses xanthine and not guanine as a substrate because XPRT lacks a catalytic acid/base found in HPRT, which necessitates that the purine base be deprotonated at neutral pH for catalysis to occur [12,31]. Xanthine is the purine base most prone to this deprotonation. XPRT's purine base discrimination suggests that it would not be a target of the alarmone (p)ppApp [32–34], which lacks the hydroxyl at C6 and a chemical moiety at C2. Indeed, we found that XPRT does not interact with ppApp (data not shown).

A common theme: PRPP motif in phosphoribosyltransferases binds (p)ppGpp

In recent years, many (p)ppGpp targets have been discovered, raising an important question of whether there are common themes in (p)ppGpp binding sites. While one common theme among many targets is that (p)ppGpp binds GTP binding sites (e.g., DNA primase and GTPases [35,36]), we recently found that (p)ppGpp binds a PRPP binding motif, rather than at a GTP binding motif, in HPRT [10]. In this work, we show that XPRT is another (p)ppGpp target that shares this PRPP binding motif, suggesting that this motif may be another common theme among many targets not harboring a GTP-binding site. This is not surprising given the structural similarity between the ribose and phosphates of PRPP and ppGpp, which would suggest that the PRPP binding motif is capable of interacting with (p)ppGpp.

XPRT is part of the PRT protein family but has evolutionarily diverged [13], illustrated by low sequence homology with either *B. subtilis* HPRT (10% identical) or *E. coli* XGPRT (12% identical). Its substrate specificity is also distinct. While *B. subtilis* HPRT uses hypoxanthine and guanine as substrates and *E. coli* XGPRT uses xanthine and guanine, *B. subtilis* XPRT is highly specific for xanthine [12,14,37]. Homologs to *B. subtilis* XPRT are found across Firmicutes and Bacteroidetes with additional representatives in Deinococcus-Thermus, Actinobacteria, and Proteobacteria (Fig. 1b). The conservation of the (p)ppGpp binding site suggests that it is likely that XPRTs across these bacteria are also regulated by (p)ppGpp (Fig. 4c). XPRT was not identified in a recent screen for (p)ppGpp binding

proteins in the firmicute *Staphylococcus aureus*, but the screen was limited to ~85% of the *S. aureus* proteome [7]. Further work is needed to verify that (p)ppGpp interacts with XPRT from this and other organisms.

There are several other recently identified (p)ppGpp targets that contain the PRPP binding motif, including the phosphoribosyltransferases XGPRT, UPRT, and PurF from *E. coli* [8–10]. All these enzymes bind PRPP as a substrate. However, not all phosphoribosyltransferases bind (p)ppGpp with the PRPP motif. The amidophosphoribosyltransferase PurF from *E. coli*, which converts PRPP and glutamine to phosphoribosylamine, binds ppGpp at an allosteric site away from the PRPP-binding active site [8]. If further examination shows that XGPRT and UPRT from *E. coli* are inhibited through (p)ppGpp binding the PRPP site, this would support a model that (p)ppGpp regulates phosphoribosyltransferases with nucleobase substrates.

Variation: Oligomeric interaction affects cooperativity, affinity, and specificity

Despite HPRT and XPRT sharing a common PRPP- and (p)ppGpp-binding motif, they display striking differences in how they interact with (p)ppGpp due to distinct oligomeric interactions (Fig. 8a). In contrast to the XPRT dimer that binds (p)ppGpp, HPRT binds (p)ppGpp as a tetramer (dimer-of-dimers) (Fig. 8b and 8c), and the differences in (p)ppGpp binding arise from diversification of oligomeric interfaces in each protein.

In one case, XPRT displays cooperative binding with (p)ppGpp likely due to a loop at its monomer-monomer interface. The monomer-monomer interfaces of HPRT and XPRT share similar overall secondary structure in an α-helix-turn-β-strand between loops I and II (Fig. 8a). However, the sequence identity at this interface has diversified, and, moreover, XPRT has an extra 10-residue bridging loop not found in HPRT (Figs. 8a and S4). The (p)ppGpp binding sites in XPRT face one another across the monomer-monomer interface (Fig. 8b), and each monomer contributes a loop that bridges the interface to interact with (p)ppGpp and form an electrostatic network of interactions (Fig. 6b). The bridging loop links the (p)ppGpp binding sites across the monomer-monomer interface, providing a likely mechanism for the cooperativity we observed in (p)ppGpp binding and inhibition (Fig. 2 and Table 1). In HPRT, on the other hand, the (p)ppGpp binding sites are on opposite sides of an HPRT dimer (Fig. 8c). HPRT lacks both the bridging loop and cooperative binding to ppGpp [10]. The electrostatic interactions provided by XPRT Arg80 in the bridging loop are instead provided by Arg165 in HPRT from within the same monomer [10]. The bridging loop is likely critical for XPRT catalysis as well as inhibition. It was previously suggested that XPRT Arg80 interacts with PRPP, and arginine residues at an analogous position in other phosphoribosyltransferases interact with PRPP [12,38,39]. Consistent with this, variants of XPRT Arg80 lack catalytic activity (Fig. S2). Although structural information of XPRT bound to PRPP is not available, Arg80's interaction with ppGpp in our structure suggests that it would interact with PRPP as well.

(p)ppGpp and PRPP's linking of XPRT monomers is likely dimerizing XPRT *in vivo*. Stable XPRT dimers have only been reported at a very high XPRT concentration of ~ 300 μM [12]. However, XPRT copy numbers in *B. subtilis* are below 15,000, so more physiologically relevant XPRT concentrations are likely below 20 μM [19–21]. At these concentrations, we

observed that XPRT was a mix of monomers and dimers (Fig. 6e), indicating that XPRT is not a dimer *in vivo* and (p)ppGpp binding dimerizes XPRT. The cooperativity is likely relevant in a physiological setting since we observed cooperativity not only in alarmone binding to XPRT but also in (p)ppGpp inhibition of XPRT activity (Fig. 2).

In addition to cooperativity, specificity and affinity of (p)ppGpp binding are also affected by diversification of interfaces between HPRT and XPRT. HPRT has an additional dimer-dimer interface that is responsible for exceedingly tight regulation of HPRT by (p)ppGpp, since the dimer interface sequesters loop II away from the binding pocket to favor inhibitor over substrate binding (Fig. 8a and 8d) [10]. In XPRT, loop II is not held by a dimer-dimer interface. Instead, it partially covers the active site, where it structurally favors alarmones with fewer 5′-phosphates, making pGpp and ppGpp more potent inhibitors of XPRT than pppGpp (Fig. 4e). The weakened binding with pppGpp may be due to the energetics required to push loop II away from this site to fit the extra phosphate. The physiological consequences of this loop II conformation are unclear and may be due to selection for enhanced binding of PRPP with its 5′-monophosphate or due to a difference in *in vivo* roles of ppGpp and pppGpp as suggested in *E. coli* [40]. Regardless, it is clear that the difference in oligomeric interfaces affects affinity and specificity of inhibitor binding.

Overall, elucidating the molecular mechanism of regulation of XPRT has highlighted the strong impact of oligomeric interaction on the evolution of diversification of enzyme regulation, affecting cooperativity, affinity, and specificity of ligand binding.

MATERIALS AND METHODS

Growth conditions and strain construction

All strains, plasmids and primers are listed in Table 3. The *B. subtilis* strains used in this study are NCIB 3610 strain background lacking the pBS32 megaplasmid. *B. subtilis* was grown on lysogeny broth (LB) and modified Spizizen agar plates supplemented with casamino acids (1X Spizizen salts [41], 1% glucose, 2 mM $MgCl_2$, 0.7 mM $CaCl_2$, 50 mM $MnCl_2$, 5 mM $FeCl_3$, 1 mM $ZnCl_2$, 2 mM thiamine, 1.5% agar, 0.1% glutamate, 0.5% casamino acids). Liquid cultures of *B. subtilis* were grown either in LB or in S7 defined medium supplemented with 1% glucose, 0.1% glutamate, and the amino acids valine, isoleucine, leucine, methionine, threonine, histidine, arginine, and tryptophan at concentrations previously reported [23,42]. Antibiotic selection was used where necessary with 10 μg/mL kanamycin and 5 μg/mL chloramphenicol for *B. subtilis*. Carbenicillin was used for *E. coli* at 100 μg/mL.

To construct a *B. subtilis xpt*::*kan* mutant (JDW4008), wild type *B. subtilis* (JDW2144) was transformed with purified genomic DNA from BKK22070 (*B. subtilis* 168 *xpt*::*kan*; *Bacillus* Genetic Stock Center). Transformants were selected on kanamycin and the genotype was confirmed with PCR using primers oJW2298 and oJW2303. To construct a (p)ppGpp^0 *xpt*::*kan* mutant (JDW4022), *B. subtilis* Δ*yjbM* Δ*ywaC* was transformed with *xpt*::*kan* linear DNA amplified from BKK22070 with primers oJW2298 and oJW2303. Transformants were selected on kanamycin and genotype was confirmed with PCR. A correct Δ*yjbM* Δ*ywaC* *xpt*::*kan* strain was transformed with purified genomic DNA from *B. subtilis* YB886 Δ*yjbM*

Δ*ywaC relA*::*cat*. Transformants were selected on chloramphenicol. Transformants were streaked on plates containing both chloramphenicol and kanamycin and genotype was confirmed with PCR (primers oJW2298/2303 for *xpt*::*kan* and primers oJW902/903 for *relA*::*cat*).

Plasmid construction and mutagenesis

Plasmids for expression of XPRT for purification were constructed by ligation independent cloning into the pLIC-trPC-HA expression vector [43]. The *xpt* gene was cloned from *B. subtilis* NCIB 3610 (GenBank accession no. CP020102). XPRT variants were created using the QuikChange Site-directed mutagenesis kit according to the manufacturer's protocol (Agilent) or using megaprimer mutagenesis [44]. Mutations were confirmed by DNA sequencing.

Protein purification

XPRT proteins were purified following a similar protocol [12]. XPRT was expressed recombinantly in *E. coli* BL21(DE3). A seed culture in LB supplemented with 100 μg/mL carbenicillin (OD ≈ 0.5) was diluted 1:50 into a batch culture of LB medium with carbenicillin. The batch culture was induced with 0.5 mM IPTG at OD_{600} ≈ 0.5 for 3 hours. Cells were pelleted by centrifugation at 10,000 x*g* for 30 min and the pellets were stored at −80 °C. Cell pellets were resuspended in buffer A [50 mM Na_2HPO_4, 150 mM NaCl, 20 mM imidazole, pH 8.0] and cells were lysed by French press. Cell debris was removed by centrifuging at 17,000 x*g* for 20 min at 4 °C. The supernatant was filtered, injected into a ÄKTA FPLC (GE Healthcare), and passed over a HisTrap FF column (GE Healthcare). XPRT was eluted with a gradient of the elution buffer [50 mM Na_2HP0_4, 150 mM NaCl, 200 mM imidazole, pH 8.0]. Fractions containing purified XPRT were determined via SDS-PAGE analysis. Fractions were collected and dialyzed into 25 mM Tris-HCl (pH 7.6) and 0.1 mM EDTA with two dialysis passages in Spectra/Por dialysis tubing (Spectrum). The concentration of purified XPRT were measured by the Bradford assay (Bio-Rad). The protein was diluted with glycerol to 20% glycerol final concentration, flash frozen, and stored at −80 °C. XPRT lacking the hexahistidine tag was purified for size exclusion chromatography by dialyzing the protein overnight with tobacco etch virus protease in 20 mM Tris-HCl (pH 7.5), 100 mM NaCl, 1 mM DTT, and 0.5 mM EDTA. The protein was dialyzed back to lysis buffer, passaged over a HisTrap FF column, and the flowthrough was collected and concentrated prior to freezing.

XPRT variants were overexpressed as above, but at 10 mL volumes for smaller scale purification. Smaller scale purification was performed with Ni-NTA spin columns (Qiagen). Cell pellets were resuspended in lysis buffer [20 mM sodium phosphate pH 8.0, 500 mM NaCl, 10 mM imidazole] with 1 mg/mL lysozyme and 375 U Benzonase endonuclease (MilliporeSigma), and cells were incubated for one hour on ice for lysis. The lysate was centrifuged at 20,000 x*g* for 15 min. The protein was purified according to the manufacturer's protocol, with the minor modification of three wash steps and three elution steps. The wash and elution buffers were identical to the lysis buffer, except with 40 mM imidazole and 500 mM imidazole, respectively. Protein purity was determined via SDS-PAGE and protein was dialyzed into 20 mM Tris-HCl pH 7.5, 100 mM NaCl, and 0.1 mM

EDTA with Slide-A-Lyzer dialysis devices (ThermoScientific). Protein was concentrated with Amicon Ultra-0.5 concentrators (MilliporeSigma), concentration was determined with the Bradford assay, and protein was frozen with liquid nitrogen for storage at −80 °C.

XPRT activity assays

XPRT activity assays were performed as previously described [12]. Briefly, reactions were carried out at 25 °C in a 100 μL mix containing 50 mM Tris-HCl (pH 7.6), 10 mM $MgCl_2$, 100 μM xanthine (MilliporeSigma), 1 mM PRPP (MilliporeSigma) and 20 nM hexahistidine-tagged XPRT. Reactions were initiated by addition of xanthine. Production of XMP was detected by monitoring absorbance at 252 nm for 10 min. A difference in extinction coefficients of 5350 $M^{-1}cm^{-1}$ was used for XMP and xanthine to convert absorbance to moles of product.

For Michaelis-Menten kinetics, reactions were performed in a UV-2401PC spectrophotometer (Shimadzu) with 100 μM xanthine and varied pppGpp and PRPP concentrations. For inhibition curves, assays were performed in a Synergy 2 plate reader (BioTek) with 50 μM xanthine and 1 mM PRPP and at variable pppGpp, ppGpp, pGpp, GTP, GDP, and GMP concentrations. (p)ppGpp was synthesized as described [24] and pGpp was a gift from José Lemos. Disodium salts of GTP (Chem Impex Int'l), GDP (Chem Impex Int'l), and GMP (MilliporeSigma) were used. The activity of XPRT variants was obtained in a Synergy 2 plate reader with 50 μM xanthine, 1 mM PRPP, and 20 nM enzyme.

Initial velocities were calculated by determining the slope of the reaction curve in R, and initial velocities of the inhibited reactions were normalized to the uninhibited initial velocity prior to fitting to the equation $Y = 1/(1 + (X / IC_{50})^n)$ to calculate IC_{50}. The Hill slope, n, was reported as the apparent Hill coefficient (n_{app}). Data fitting was performed using GraphPad Prism v5.02.

Radiolabeled ^{32}P-(p)ppGpp synthesis and purification

[5′-α-^{32}P]-pppGpp was synthesized from [α-^{32}P]-GTP (Perkin Elmer) and ATP using Rel_{Seq} (1–385) and purified using a HiTrap QFF anion exchange column (GE Healthcare) as previously described [10,45]. To synthesize [5′-α-^{32}P]-ppGpp, 75 mM NH_4Cl from a 4 M stock was added to a completed ^{32}P-pppGpp reaction followed by the addition of 37.5 μg/mL *E. coli* GppA (GppA purified according to [40]). The reaction was continued for an additional hour prior to anion exchange purification. [5′-α-^{32}P]-pGpp was purified as described [17].

DRaCALA

Differential radial capillary action of ligand assay (DRaCALA) utilizes the ability of nitrocellulose to separate free ligand from the protein-ligand complex and was used to detect and quantify direct binding of (p)ppGpp to XPRT [15]. Binding assays were performed on purified hexahistidine-tagged *B. subtilis* XPRT and XPRT variants similarly as described before [10]. Reactions were carried out in a 15–20 μL reaction mixture with protein diluted in 20 mM HEPES pH 8, 100 mM NaCl, and 10 mM $MgCl_2$. Radiolabeled (p)ppGpp was added at a final concentration of 1:50–1:100 of the first elution fraction from synthesis.

Reactions were pipetted or shaken to mix, incubated at room temperature for 10 min, and 2 μL of each reaction was spotted onto Protran BA85 nitrocellulose (GE Healthcare) via pipette or a replicator pinning tool (V&P Scientific, Inc.). After drying for at least 20 min, the nitrocellulose was exposed to a phosphorscreen and scanned with a Typhoon phosphorimager (GE Healthcare). Spot intensity was quantified using ImageJ software. Fraction ^{32}P-(p)ppGpp bound was calculated and edge effect was corrected as previously described [15]. Data were analyzed in GraphPad Prism v5.02 and binding curves were fitted to the equation $Y = (B_{max} \times X^h) / (K_d{}^h + X^h)$, where h is the Hill coefficient (n_H).

Determination of XPRT-ppGpp costructure

PDB ID **1Y0B** was previously deposited by the Midwest Center for Structural Genomics. The crystals were reported to be obtained with hanging drop vapor diffusion with bis-Tris pH 5.5, NaCl, and PEG 3350 as the crystallization condition (concentrations not provided). The coordinate and structure factor files for PDB ID **1Y0B** were downloaded from the PDB website. Electron density maps ($2F_o$-F_c and F_o-F_c) were calculated and displayed in COOT [46]; these clearly showed density for the 5′ portion of ppGpp that was not fit in the deposited structure. Real space refinement in COOT gave acceptable fits in each of the 4 instances of ppGpp. Phenix refine [47] was used to refine the structure with the full ppGpp to R_{free} = 15.3 and R_{work} = 20.8. The fit of ppGpp was further examined in COOT. The sodium sites in the 3′-phosphates were checked with CheckMyMetal [48] and are not magnesium sites. Bond lengths to the water in between the 5′-phosphates indicate the possibility that a sodium ion binds the 5′-phosphates.

Differential scanning fluorimetry

Differential scanning fluorimetry was performed as previously described [49]. Protein (10 μM) was combined with 5X Sypro Orange dye (ThermoFisher, 5000X stock) in a buffer diluted from a 5X stock (final 10 mM HEPES pH 8, 100 mM NaCl, and 10 mM $MgCl_2$). The protein and dye were incubated at 25 °C to 90 °C (1 °C/min ramp) using a Bio-Rad CFX Connect Real-time thermocycler. Measurements were taken every minute. T_m values were determined as the minimum of the first derivative of the melting curves as provided by the CFX Manager software.

Size exclusion chromatography

Size exclusion chromatography was performed with an AktaPure FPLC and Superose 12 10/300 GL column (GE Healthcare) with a flow rate of 0.25 mL/min. The mobile phase was 20 mM HEPES pH 8, 300 mM NaCl, and 10 mM $MgCl_2$. ppGpp was added to the mobile phase at a final concentration of 35 μM. The column was equilibrated with at least one column volume of buffer prior to addition of protein. The predicted dimer and monomer retention volumes were calculated from the molecular weight of untagged XPRT using a previously published standard curve for this column [10] [log(molecular weight) = −0.2575 × retention volume + 7.821]. With a molecular weight of 21038 Da, the predicted retention volumes are 13.58 for an XPRT monomer and 12.41 for an XPRT dimer. The A_{280} (mAU) curves were normalized to have a baseline near zero.

B. subtilis viability assays

Strains JDW2144, JDW2231, JDW4008, and JDW4022 were used to assess viability with xanthine. A single colony of each strain was resuspended in S7 medium supplemented with the amino acids VILMTH and spread on Spizizen agar plates supplemented with casamino acids. The strains were grown until small colonies formed (≈16 hrs at 30 °C). Cultures were collected from the overnight plates with S7+VILMTH, diluted to OD_{600} 0.01 in S7+VILMTH and grown until OD_{600} ≈ 0.2. A t=0 sample was taken, and the remaining culture was divided for addition of 1 mM xanthine (from 100 mM stock) or water. Samples were taken at 30, 60, and 120 min. Ten fold dilutions of cultures were plated on LB for quantification of CFU/mL. Guanine treatment (1 mM final) of JDW2144 and JDW2231 followed the same protocol with a sample taken prior to treatment (t=0) and 60 min after treatment.

Thin layer chromatography

Thin layer chromatography was performed as described [27,50]. Wild type (JDW2144) and (p)ppGpp^0 (JDW2231) *B. subtilis* were washed from overnight plates and diluted in limited phosphate (1/10 phosphate concentration) S7 medium supplemented with the amino acids VILMTHRW. Cultures were grown until OD_{600} ≈ 0.02 and labeled with 50 μCi/ml ^{32}P-orthophosphate (900 mCi/mmol; PerkinElmer). When OD_{600} reached 0.2–0.4, cultures were treated with 1 mM xanthine for 30 min. Nucleotides were extracted by mixing 75 μL of culture with 15 μL of cold 2 N formic acid and incubating on ice for at least 20 min. Extracts were centrifuged at 14,000 x*g* for at least 15 min at 4 °C. Two microliters of supernatant were spotted on PEI cellulose TLC plates (MilliporeSigma) and developed in 0.85 M KH_2PO_4 pH 3.4. The TLC plates were then exposed to a phosphorscreen and scanned by a Typhoon phosphorimager.

Protein alignments

XPRT proteins were selected from representative bacterial species by searching for EC 2.4.2.22 in UniProt. Proteins were chosen that were at least 190 residues since the *B. subtilis* XPRT homologs are longer than either HPRTs (~180 aa) or XGPRTs (~150 aa). Proteins were aligned in MEGA X with MUSCLE. (p)ppGpp-interacting residues were determined with LigPlot, and the positions for these residues were selected from the alignment. The frequency logo was generated from the aligned binding residues in WebLogo (https://weblogo.berkeley.edu/logo.cgi). Percent identities between PRT homologs was determined by aligning the proteins in PROMALS3D with PDB ID **1Y0B**, PDB ID **6D9S**, and PDB ID **1A97** used for *B. subtilis* XPRT, *B. subtilis* HPRT, and *E. coli* XGPRT, respectively [51]. Percent identities were calculated as fraction of identical residues across the whole alignment, including gaps.

XPRT conservation

16S rRNA sequences for 41 bacterial species representing six phyla were downloaded from NCBI or the Ribosomal Database Project [52]. 18S rRNA sequences from three eukaryotic species were downloaded from NCBI. Sequences were aligned with CLUSTAL in MEGA X [53]. MEGA X's model testing tool was used to select Tamura-Nei model with gamma

distributed categories as the best fitting model. A phylogenetic tree was constructed in MEGA X with this model and 100 bootstrap replicates. The presence of XPRT in each species was determined by BLASTing *B. subtilis* XPRT against each species' proteome. The tree was modified and annotated using the R package ggtree [54].

Supplementary Material

Refer to Web version on PubMed Central for supplementary material.

ACKNOWLEDGMENTS

We thank the Wang lab for discussion and critical reading of this manuscript, and we thank the reviewers for their helpful suggestions. PDB ID **1Y0B** was deposited by the Midwest Center for Structural Genomics, which was funded by NIH GM62414. This work was funded by NIH R35 GM127088 and R01 GM084003 to J. D. W., and B. W. A. was supported by NSF GRFP DGE-1256259.

REFERENCES

[1]. Dakora FD, Phillips D. a., Root exudates as mediators of mineral acquisition in low-nutrient environments, Plant Soil. 245 (2002) 35–47. 10.1023/A:1020809400075.

[2]. Traut TW, Physiological concentrations of purines and pyrimidines, Mol. Cell. Biochem 140 (1994) 1–22. 10.1007/BF00928361. [PubMed: 7877593]

[3]. Rolfes RJ, Regulation of purine nucleotide biosynthesis: in yeast and beyond, Biochem. Soc. Trans 34 (2006) 786–790. 10.1042/BST0340786. [PubMed: 17052198]

[4]. Nyhan WL, Nucleotide synthesis via salvage pathway, in: ELS, John Wiley & Sons, Inc., 2014: pp. 1–7. 10.1038/npg.els.0003909.

[5]. Kriel A, Bittner AN, Kim SH, Liu K, Tehranchi AK, Zou WY, Rendon S, Chen R, Tu BP, Wang JD, Direct regulation of GTP homeostasis by (p)ppGpp: a critical component of viability and stress resistance., Mol. Cell 48 (2012) 231–241. 10.1016/j.molcel.2012.08.009. [PubMed: 22981860]

[6]. Hochstadt-Ozer J, Cashel M, The regulation of purine utilization in bacteria: Inhibition of purine phosphoribosyltransferase activities and purine uptake in isolated membrane vesicles by guanosine tetraphosphate, J. Biol. Chem 247 (1972) 7067–7072. [PubMed: 4343167]

[7]. Corrigan RM, Bellows LE, Wood A, Gründling A, ppGpp negatively impacts ribosome assembly affecting growth and antimicrobial tolerance in Gram-positive bacteria, Proc. Natl. Acad. Sci. U. S. A 113 (2016) 201522179 10.1073/pnas.1522179113.

[8]. Wang B, Dai P, Ding D, Del Rosario A, Grant RA, Pentelute BL, Laub MT, Del Rosario A, Grant RA, Pentelute BL, Laub MT, Affinity-based capture and identification of protein effectors of the growth regulator ppGpp, Nat. Chem. Biol 15 (2018) 141–150. 10.1038/s41589-018-0183-4. [PubMed: 30559427]

[9]. Zhang Y, Zbornikova E, Rejman D, Gerdes K, Novel (p)ppGpp binding and metabolizing proteins of *Escherichia coli*, MBio. 9 (2018) e02188–17. 10.1128/mBio.02188-17. [PubMed: 29511080]

[10]. Anderson BW, Liu K, Wolak C, Dubiel K, She F, Satyshur KA, Keck JL, Wang JD, Evolution of (p)ppGpp-HPRT regulation through diversification of an allosteric oligomeric interaction, Elife. 8 (2019) e47534 10.1017/CBO9781107415324.004. [PubMed: 31552824]

[11]. Christiansen LC, Schou S, Nygaard P, Saxild HH, Xanthine metabolism in *Bacillus subtilis*: Characterization of the *xpt- pbuX* operon and evidence for purine- and nitrogen-controlled expression of genes involved in xanthine salvage and catabolism, J. Bacteriol 179 (1997) 2540–2550. [PubMed: 9098051]

[12]. Arent S, Kadziola A, Larsen S, Neuhard J, Jensen KF, The extraordinary specificity of xanthine phosphoribosyltransferase from *Bacillus subtilis* elucidated by reaction kinetics, ligand binding, and crystallography, Biochemistry. 45 (2006) 6615–27. 10.1021/bi060287y. [PubMed: 16716072]

[13]. Hove-Jensen B, Andersen KR, Kilstrup M, Martinussen J, Switzer RL, Willemoes M, Phosphoribosyl diphosphate (PRPP): biosynthesis, enzymology, utilization, and metabolic significance, Microbiol. Mol. Biol. Rev 81 (2017) e00040–16. [PubMed: 28031352]

[14]. Vos S, Parry RJ, Burns MR, de Jersey J, Martin JL, Structures of free and complexed forms of *Escherichia coli* xanthine-guanine phosphoribosyltransferase, J. Mol. Biol 282 (1998) 875–889. [PubMed: 9743633]

[15]. Roelofs KG, Wang J, Sintim HO, Lee VT, Differential radial capillary action of ligand assay for high-throughput detection of protein-metabolite interactions, Proc. Natl. Acad. Sci. U. S. A 108 (2011) 15528–33. 10.1073/pnas.1018949108. [PubMed: 21876132]

[16]. Gaca AO, Kudrin P, Colomer-Winter C, Beljantseva J, Liu K, Anderson B, Wang JD, Rejman D, Potrykus K, Cashel M, Hauryliuk V, Lemos JA, From (p)ppGpp to (pp)pGpp: Characterization of regulatory effects of pGpp synthesized by the small alarmone synthetase of *Enterococcus faecalis*, J. Bacteriol 197 (2015) 2908–2919. 10.1128/JB.00324-15. [PubMed: 26124242]

[17]. Yang J, Anderson BW, Turdiev A, Turdiev H, Stevenson DM, Systemic characterization of pppGpp, ppGpp and pGpp targets in *Bacillus* reveal SatA converts (p)ppGpp to pGpp to regulate alarmone composition and signaling, BioRxiv. [Preprint] (2020).

[18]. Krissinel E, Henrick K, Inference of macromolecular assemblies from crystalline state, J. Mol. Biol 372 (2007) 774–797. 10.1016/j.jmb.2007.05.022. [PubMed: 17681537]

[19]. Maass S, Sievers S, Zuhlke D, Kuzinski J, Sappa PK, Muntel J, Hessling B, Bernhardt J, Sietmann R, Volker U, Hecker M, Becher D, Efficient, global-scale quantification of absolute protein amounts by integration of targeted mass spectrometry and two-dimensional gel-based proteomics, Anal. Chem 83 (2011) 2677–2684. 10.1021/ac1031836. [PubMed: 21395229]

[20]. Maass S, Wachlin G, Bernhardt J, Eymann C, Fromion V, Riedel K, Becher D, Hecker M, Highly precise quantification of protein molecules per cell during stress and starvation responses in *Bacillus subtilis*, Mol. Cell. Proteomics 13 (2014) 2260–2276. 10.1074/mcp.M113.035741. [PubMed: 24878497]

[21]. Muntel J, Fromion V, Goelzer A, Maass S, Mäder U, Büttner K, Hecker M, Becher D, Comprehensive absolute quantification of the cytosolic proteome of *Bacillus subtilis* by data independent, parallel fragmentation in liquid chromatography/mass spectrometry (LC/MSE), Mol. Cell. Proteomics 13 (2014) 1008–1019. 10.1074/mcp.M113.032631. [PubMed: 24696501]

[22]. Krásný L, Gourse RL, An alternative strategy for bacterial ribosome synthesis: *Bacillus subtilis* rRNA transcription regulation, EMBO J. 23 (2004) 4473–83. 10.1038/sj.emboj.7600423. [PubMed: 15496987]

[23]. Kriel A, Brinsmade SR, Tse JL, Tehranchi AK, Bittner AN, Sonenshein AL, Wang JD, GTP dysregulation in *Bacillus subtilis* cells lacking (p)ppGpp results in phenotypic amino acid auxotrophy and failure to adapt to nutrient downshift and regulate biosynthesis genes, J. Bacteriol 196 (2014) 189–201. 10.1128/JB.00918-13. [PubMed: 24163341]

[24]. Liu K, Myers AR, Pisithkul T, Claas KR, Satyshur KA, Amador-Noguez D, Keck JL, Wang JD, Molecular mechanism and evolution of guanylate kinase regulation by (p)ppGpp, Mol. Cell 57 (2015) 735–749. 10.1016/j.molcel.2014.12.037. [PubMed: 25661490]

[25]. Gallant J, Irr J, Cashel M, The mechanism of amino acid control of guanylate and adenylate biosynthesis, J. Biol. Chem 246 (1971) 5812–5816. [PubMed: 4938039]

[26]. Lopez JM, Dromerick A, Freese E, Response of guanosine 5'-triphosphate concentration to nutritional changes and its significance for *Bacillus subtilis* sporulation, J. Bacteriol 146 (1981) 605–613. https://doi.org/0021-9193/81/050605-09. [PubMed: 6111556]

[27]. Bittner AN, Kriel A, Wang JD, Lowering GTP level increases survival of amino acid starvation but slows growth rate for *Bacillus subtilis* cells lacking (p)ppGpp, J. Bacteriol 196 (2014) 2067–76. 10.1128/JB.01471-14. [PubMed: 24682323]

[28]. Beaman TC, Hitchins AD, Ochi K, Endo T, Freese E, Specificity and control of uptake of purines and other compounds in *Bacillus subtilis*, J. Bacteriol 156 (1983) 1107–1117. [PubMed: 6417108]

[29]. Townsend MH, Felsted AM, Burrup W, Robison RA, O'Neill KL, Examination of hypoxanthine guanine phosphoribosyltransferase as a biomarker for colorectal cancer patients, Mol. Cell. Oncol 5 (2018) 1–13. 10.1080/23723556.2018.1481810.

[30]. Hochstadt J, Magasanik B, The role of the membrane in the utilization of nucleic acid precursor, Crit. Rev. Biochem. Mol. Biol 2 (1974) 259–310. 10.3109/10409237409105449.

[31]. Xu Y, Grubmeyer C, Catalysis in human hypoxanthine-guanine phosphoribosyltransferase: Asp 137 acts as a general acid/base, Biochemistry. 37 (1998) 4114–4124. 10.1021/bi972519m. [PubMed: 9521733]

[32]. Ahmad S, Wang B, Walker MD, Tran HKR, Stogios PJ, Savchenko A, Grant RA, McArthur AG, Laub MT, Whitney JC, An interbacterial toxin inhibits target cell growth by synthesizing (p)ppApp, Nature. 575 (2019) 674–678. 10.1038/s41586-019-1735-9. [PubMed: 31695193]

[33]. Sobala M, Bruhn-Olszewska B, Cashel M, Potrykus K, *Methylobacterium extorquens* RSH enzyme synthesizes (p)ppGpp and pppApp *in vitro* and *in vivo*, and leads to discovery of pppApp synthesis in *Escherichia coli*, Front. Microbiol 10 (2019) 1–13. 10.3389/fmicb.2019.00859. [PubMed: 30728808]

[34]. Rhaese HJ, Hoch JA, Groscurth R, Studies on the control of development: isolation of *Bacillus subtilis* mutants blocked early in sporulation and defective in synthesis of highly phosphorylated nucleotides, Proc. Natl. Acad. Sci. U. S. A 74 (1977) 1125–1129. 10.1073/pnas.74.3.1125. [PubMed: 403525]

[35]. Rymer RU, Solorio FA, Tehranchi AK, Chu C, Corn JE, Keck JL, Wang JD, Berger JM, Binding mechanism of metal·NTP substrates and stringent-response alarmones to bacterial DnaG-type primases, Structure. 20 (2012) 1478–1489. 10.1016/j.str.2012.05.017. [PubMed: 22795082]

[36]. Bennison DJ, Irving SE, Corrigan RM, The Impact of the Stringent Response on TRAFAC GTPases and Prokaryotic Ribosome Assembly., Cells. 8 (2019). 10.3390/cells8111313.

[37]. Endo T, Uratani B, Freese E, Purine salvage pathways of *Bacillus subtilis* and effect of guanine on growth of GMP reductase mutants, J. Bacteriol 155 (1983) 169–179. [PubMed: 6408059]

[38]. Shi W, Sarver AE, Wang CC, Tanaka KSE, Almo SC, Schramm VL, Closed site complexes of adenine phosphoribosyltransferase from *Giardia lamblia* reveal a mechanism of ribosyl migration, J. Biol. Chem 277 (2002) 39981–39988. 10.1074/jbc.M205596200. [PubMed: 12171925]

[39]. Scapin G, Ozturk DH, Grubmeyer C, Sacchettini JC, The crystal structure of the orotate phosphoribosyltransferase complexed with orotate and a-D-5-phosphoribosyl-1-pyrophosphate, Biochemistry. 34 (1995) 10744–10754. 10.1021/bi00034a006. [PubMed: 7545004]

[40]. Mechold U, Potrykus K, Murphy H, Murakami KS, Cashel M, Differential regulation by ppGpp versus pppGpp in *Escherichia coli*, Nucleic Acids Res. 41 (2013) 6175–6189. 10.1093/nar/gkt302. [PubMed: 23620295]

[41]. Spizizen J, Transformation of biochemically deficient strains of *Bacillus subtilis* by deoxyribonucleate, Proc. Natl. Acad. Sci 44 (1958) 1072–1078. 10.1073/pnas.44.10.1072. [PubMed: 16590310]

[42]. Vasantha N, Freese E, Enzyme changes during *Bacillus subtilis* sporulation caused by deprivation of guanine nucleotides, J. Bacteriol 144 (1980) 1119–1125. [PubMed: 6777366]

[43]. Stols L, Gu M, Dieckman L, Raffen R, Collart FR, Donnelly MI, A new vector for high-throughput, ligation-independent cloning encoding a tobacco etch virus protease cleavage site, Protein Expr. Purif 25 (2002) 8–15. 10.1006/prep.2001.1603. [PubMed: 12071693]

[44]. Kirsch RD, Joly E, An improved PCR-mutagenesis strategy for two-site mutagenesis or sequence swapping between related genes, Nucleic Acids Res. 26 (1998) 1848–1850. 10.1093/nar/26.7.1848. [PubMed: 9512562]

[45]. Mechold U, Murphy H, Brown L, Cashel M, Intramolecular regulation of the opposing (p)ppGpp catalytic activities of Rel$_{Seq}$, the Rel/Spo enzyme from *Streptococcus equisimilis*, J. Bacteriol 184 (2002) 2878–2888. 10.1128/JB.184.11.2878. [PubMed: 12003927]

[46]. Emsley P, Cowtan K, Coot: model-building tools for molecular graphics, Acta Crystallogr. Sect. D Biol. Crystallogr 60 (2004) 2126–2132. 10.1107/S0907444904019158. [PubMed: 15572765]

[47]. Adams PD, Afonine PV, Bunkoczi G, Chen VB, Davis IW, Echols N, Headd JJ, Hung L-W, Kapral GJ, Grosse-Kunstleve RW, McCoy AJ, Moriarty NW, Oeffner R, Read RJ, Richardson DC, Richardson JS, Terwilliger TC, Zwart PH, PHENIX: a comprehensive Python-based system for macromolecular structure solution, Acta Crystallogr. Sect. D Biol. Crystallogr 66 (2010) 213–221. 10.1107/S0907444909052925. [PubMed: 20124702]

[48]. Zheng H, Cooper DR, Porebski PJ, Shabalin IG, Handing KB, Minor W, CheckMyMetal: A macromolecular metal-binding validation tool, Acta Crystallogr. Sect. D Struct. Biol 73 (2017) 223–233. 10.1107/S2059798317001061. [PubMed: 28291757]

[49]. Niesen FH, Berglund H, Vedadi M, The use of differential scanning fluorimetry to detect ligand interactions that promote protein stability, Nat. Protoc 2 (2007) 2212–2221. 10.1038/nprot.2007.321. [PubMed: 17853878]

[50]. Schneider DA, Murray HD, Gourse RL, Measuring control of transcription initiation by changing concentrations of nucleotides and their derivatives, Methods Enzymol. 370 (2003) 606–617. 10.1016/S0076-6879(03)70051-2. [PubMed: 14712679]

[51]. Pei J, Kim B, V Grishin N, PROMALS3D: a tool for multiple protein sequence and structure alignments, Nucleic Acids Res. 36 (2008) 2295–2300. 10.1093/nar/gkn072. [PubMed: 18287115]

[52]. Cole JR, Wang Q, Fish JA, Chai B, Mcgarrell DM, Sun Y, Brown CT, Porrasalfaro A, Kuske CR, Tiedje JM, Ribosomal Database Project: data and tools for high throughput rRNA analysis, Nucleic Acids Res. 42 (2014) 633–642. 10.1093/nar/gkt1244.

[53]. Kumar S, Stecher G, Li M, Knyaz C, Tamura K, MEGA X: Molecular evolutionary genetics analysis across computing platforms, Mol. Biol. Evol 35 (2018) 1547–1549. 10.1093/molbev/msy096. [PubMed: 29722887]

[54]. Yu G, Smith DK, Zhu H, Guan Y, Lam TTY, GGTREE: an R package for visualization and annotation of phylogenetic trees with their covariates and other associated data, Methods Ecol. Evol 8 (2017) 28–36. 10.1111/2041-210X.12628.

[55]. Konkol MA, Blair KM, Kearns DB, Plasmid-encoded ComI inhibits competence in the ancestral 3610 strain of *Bacillus subtilis*, J. Bacteriol 195 (2013) 4085–4093. 10.1128/JB.00696-13. [PubMed: 23836866]

[56]. Fung DK, Barra JT, Schroeder JW, Ying D, Wang JD, A shared alarmone-GTP switch underlies triggered and spontaneous persistence, BioRxiv. [Preprint] (2020).

Highlights

- The purine salvage enzyme XPRT uses xanthine and PRPP for efficient GTP synthesis.
- The alarmones pppGpp, ppGpp, and pGpp bind XPRT's PRPP binding motif.
- XPRT is potently inhibited by pGpp and ppGpp and moderately inhibited by pppGpp.
- XPRT dimers cooperatively bind (p)ppGpp using bridging loops between two monomers.
- Regulation of XPRT protects cell viability during growth with environmental xanthine.

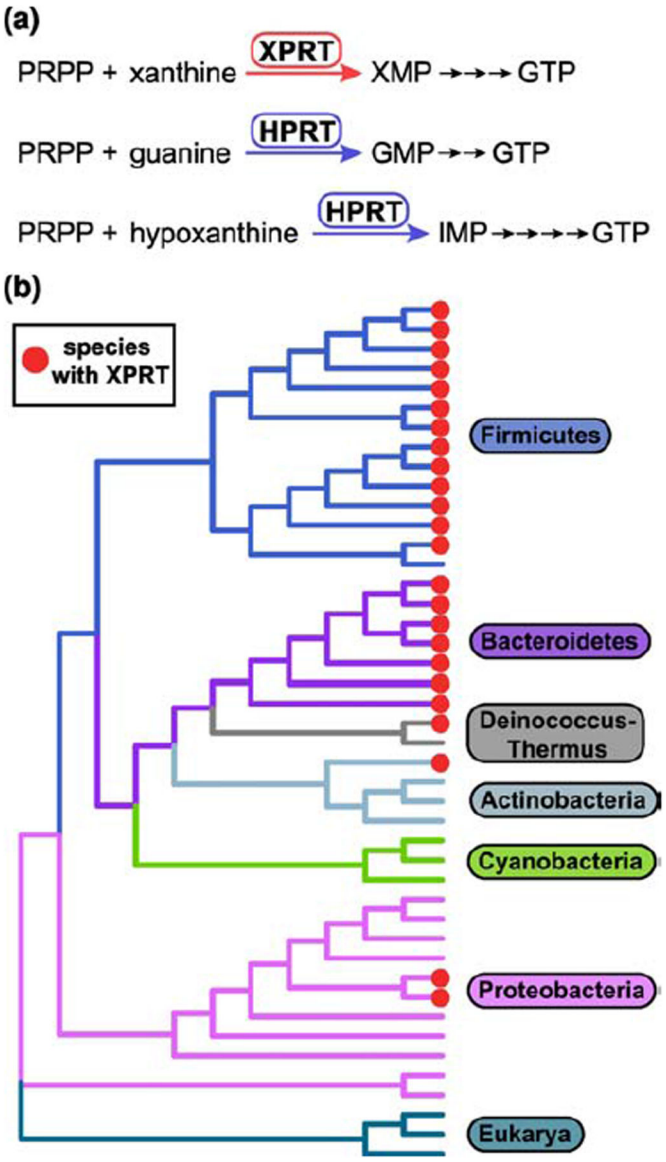

Figure 1. XPRT is a purine salvage enzyme conserved in Firmicutes and Bacteroidetes.

(a) The purine salvage enzyme XPRT catalyzes the conversion of PRPP and nucleobase xanthine to the GTP precursor XMP. XPRT is homologous to the salvage enzyme HPRT that converts guanine or hypoxanthine to GMP or IMP. These salvage reactions are efficient pathways for GTP synthesis. **(b)** Cladogram constructed from 16S rRNA sequences from 41 bacterial species representing six bacterial phyla. Three eukaryotic 18S rRNA sequences included as the outgroup. Bacterial species containing XPRT are marked with red circles.

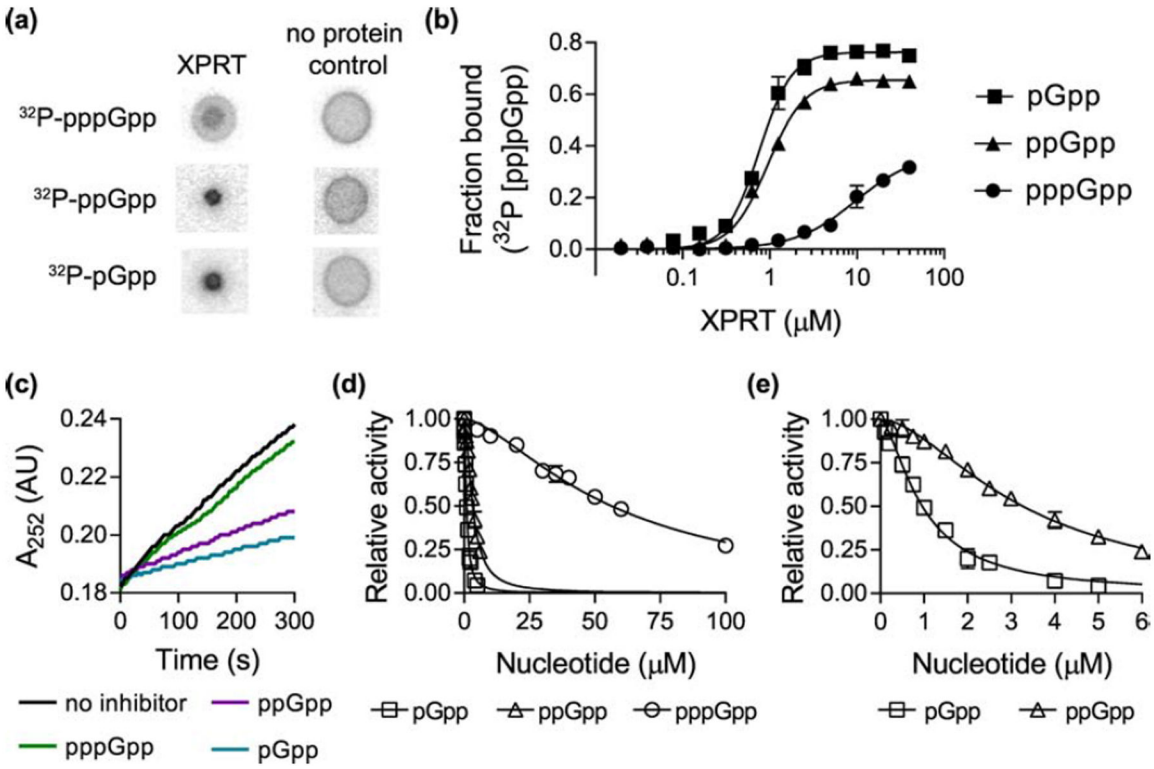

Figure 2. pppGpp, ppGpp, and pGpp bind and inhibit the activity of XPRT.

(a) Representative DRaCALA data showing the interaction between 20 μM *B. subtilis* XPRT and ^{32}P-pppGpp, ^{32}P-ppGpp, and ^{32}P-pGpp. The amount of radioactivity in the inner spot is a measure of the interaction. **(b)** Binding curves for ^{32}P-pGpp, ^{32}P-ppGpp, and ^{32}P-pppGpp with varying XPRT concentrations. Binding determined by DRaCALA. Data are fitted to a single-site binding equation with the Hill coefficient. **(c)** Representative data showing first-order kinetic curves of XPRT activity with no inhibitor or with 1.56 μM pppGpp, ppGpp, or pGpp. Production of XMP measured as increased A_{252}. Activity determined with 1 mM PRPP and 50 μM xanthine as substrates. **(d)** Relative activity of XPRT at varied concentrations of pppGpp, ppGpp, and pGpp. **(e)** Same data from (d) shown with a different X-axis scale to show the inhibition curves for ppGpp and pGpp. In (d) and (e), data are fitted to a dose-response equation with the Hill coefficient. See Table 1 for binding and inhibition parameters. Error bars represent SEM of at least three replicates.

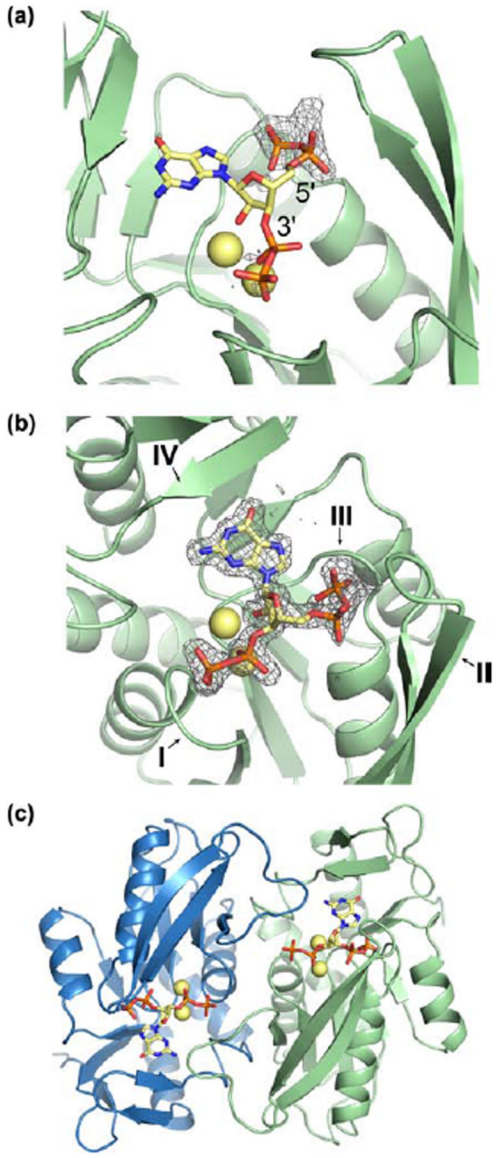

Figure 3. Costructure of *B. subtilis* XPRT and ppGpp.

(a) Refinement of *B. subtilis* XPRT crystallized with ppGpp (PDB ID **1Y0B**). The deposited structure lacked 5'-phosphates, but 5'-phosphates fit the F_o-F_c difference density (contoured to 2.5 σ) at the 5'-carbon. In A–C, yellow spheres are Na^+ ions crystallized with ppGpp. **(b)** ppGpp binding an XPRT monomer. Omit difference density shown contoured to 2.5 σ. I–IV refer to the four loops of the PRT active site. **(c)** Biological dimer of XPRT-ppGpp as predicted by PISA analysis. Each monomer in the dimer binds one ppGpp molecule.

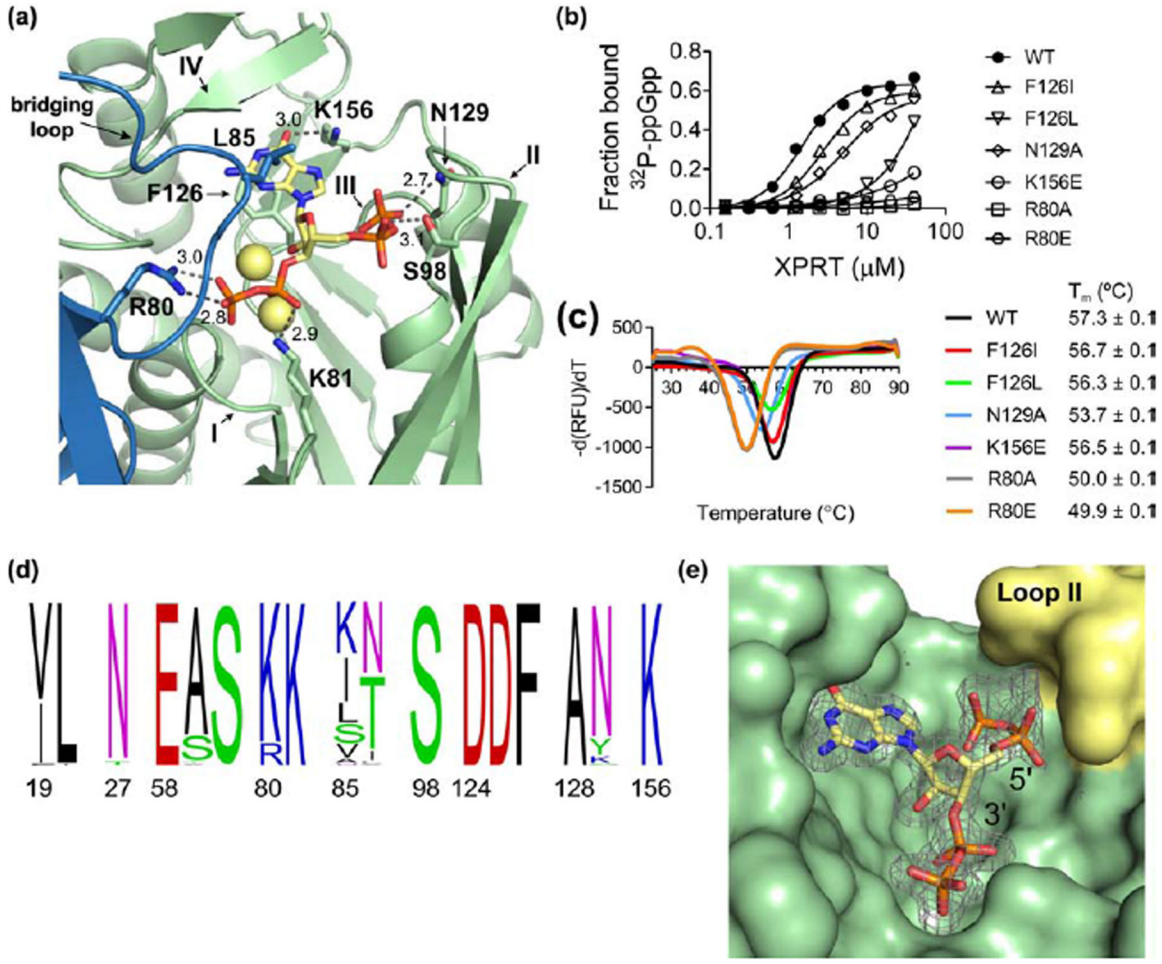

Figure 4. (p)ppGpp binds the conserved XPRT active site, and a flexible loop covering the pocket differentiates between pppGpp and ppGpp/pGpp.

(a) Select residues involved in the ppGpp-XPRT interaction. Hydrogen bonding shown as dotted lines and is measured in Å. The blue protein is the adjoining monomer in the structure. Yellow spheres are Na^+ ions. **(b)** DRaCALA of *B. subtilis* XPRT active site variants shows that ^{32}P-ppGpp binding is weakened by altering these residues. Points are mean of triplicate for all but F126L (duplicate). Error bars represent SEM for triplicate and range for duplicate. Error bars may be smaller than the height of the symbols. **(c)** Derivative curves from differential scanning fluorimetry of XPRT variants. Curves show the mean of triplicate reactions. Melting temperature (T_m) is the mean of three replicates ± SEM. **(d)** Frequency logo of the ppGpp-binding residues from 62 bacterial XPRTs. Numbering is according to *B. subtilis* XPRT. Residues are colored according to their class. Logo generated using WebLogo (UC Berkeley). **(e)** Surface view of the ppGpp binding pocket on XPRT. Omit difference density for ppGpp is shown contoured at 2.5 σ. The compression around the 5'-phosphates caused by loop II (yellow) may be responsible for weaker interaction with pppGpp than ppGpp/pGpp.

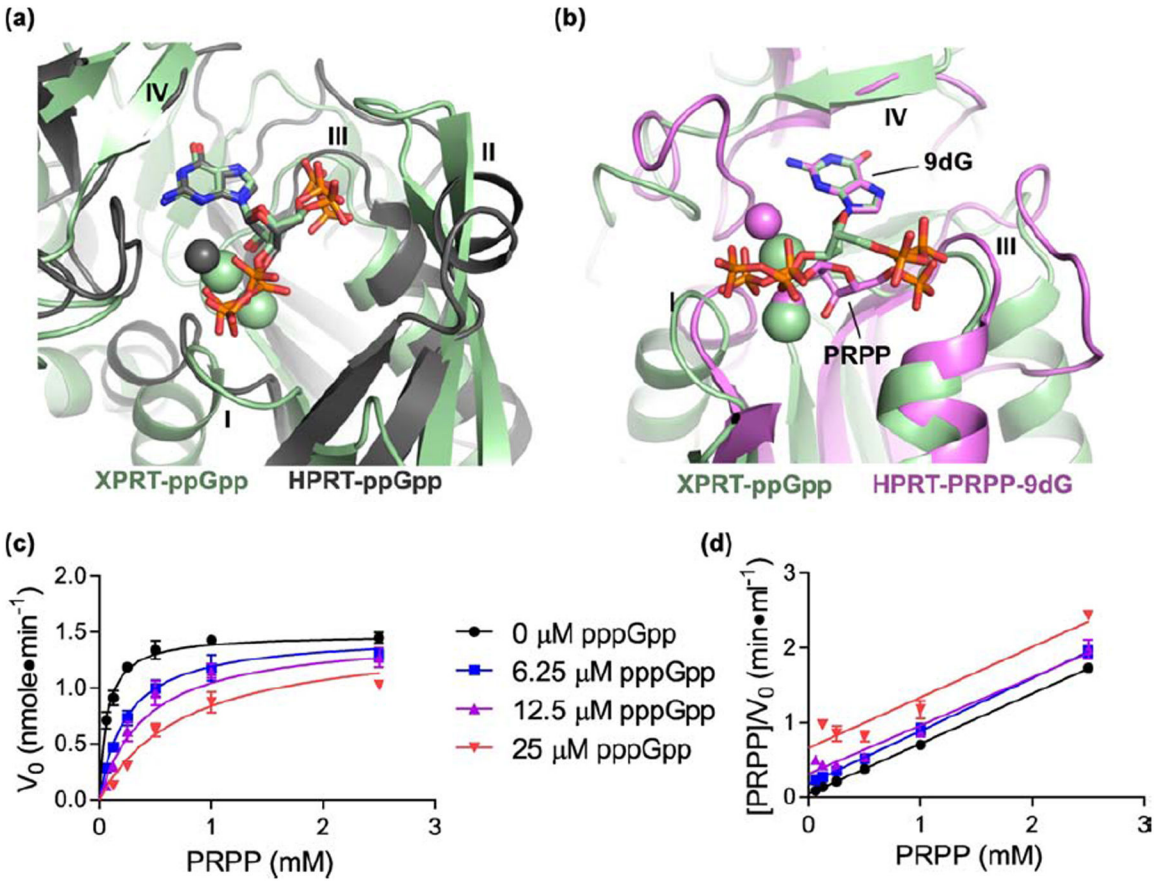

Figure 5. pppGpp competes with PRPP to inhibit XPRT.

(a) Overlay of XPRT-ppGpp (green) and ppGpp-bound *B. anthracis* Hpt-1 (gray; PDB ID **6D9S**). Alignment based on ppGpp molecules. Gray sphere is Mg^{2+} crystallized with HPRT-ppGpp. Green spheres are Na^{+} crystallized with XPRT-ppGpp. **(b)** Overlay of XPRT-ppGpp (green) and substrates-bound *B. anthracis* Hpt-1 (pink; PDB ID **6D9R**). Alignment based on guanine of ppGpp and 9-deazaguanine (9dG) of substrates. ppGpp binds the XPRT active site and overlaps with substrate binding. Loop II for both proteins hidden for clarity. Pink spheres are Mg^{2+} crystallized with HPRT-ppGpp. Green spheres are Na^{+} crystallized with XPRT-ppGpp. **(c)** Initial velocities of *B. subtilis* XPRT at varied pppGpp and PRPP concentrations. Data are fitted to a global competitive inhibition model with a K_i of 2.5 μM. **(d)** Hanes-Woolf transformation from the data in (c). Equivalent slopes indicate equivalent maximum velocities at each pppGpp concentration. Error bars represent SEM of at least three replicates.

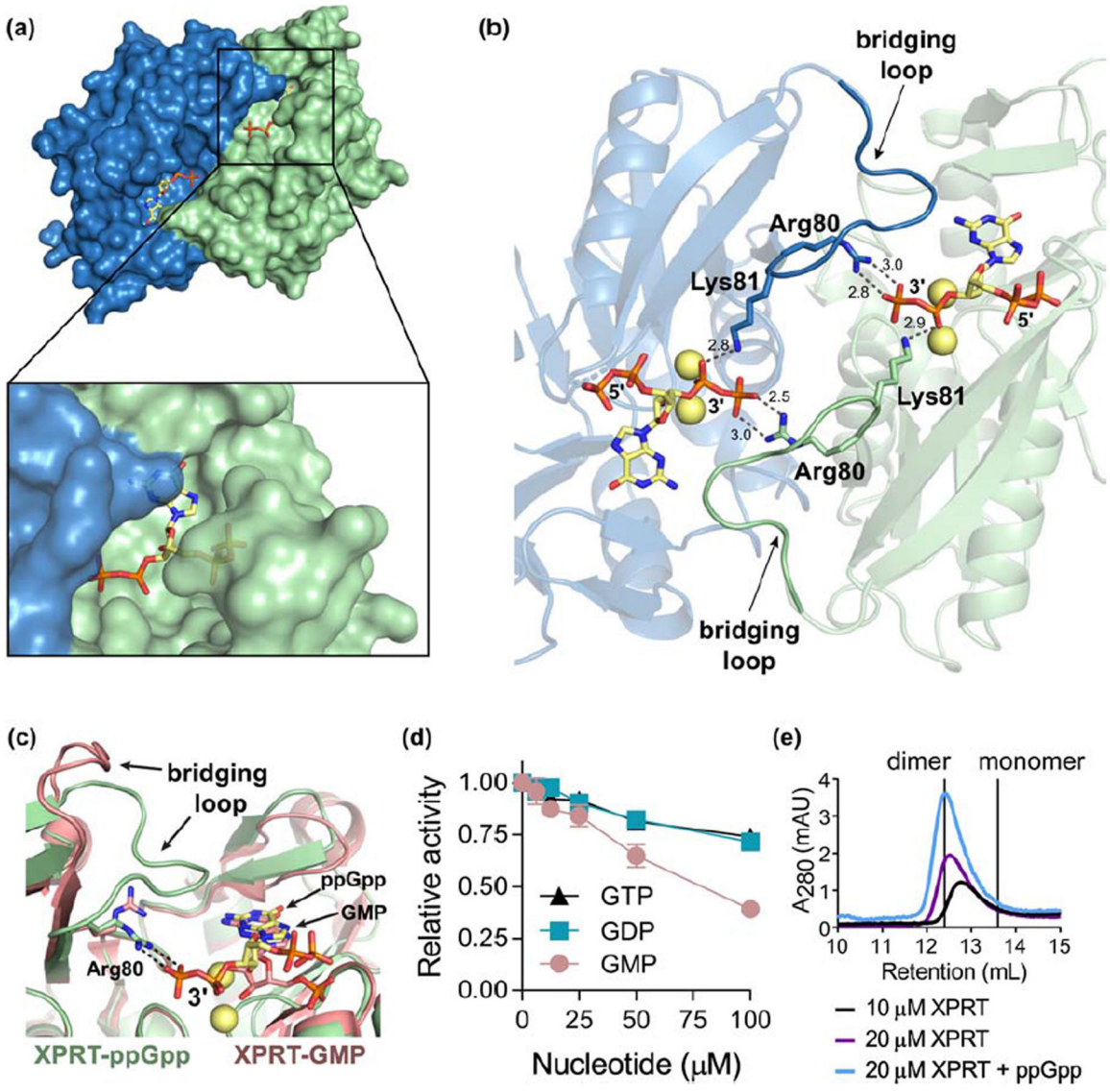

Figure 6. (p)ppGpp stabilizes XPRT dimers by establishing electrostatic interactions bridging the monomer-monomer interface.

(a) *B. subtilis* XPRT dimer bound to ppGpp. Inset shows how ppGpp is covered by the second monomer. **(b)** Arg80 and Lys81 interact with the 3'-phosphates of ppGpp to create a network of electrostatic interactions across the monomer-monomer interface. Residues 80–89 comprise the bridging loop (opaque) that interacts with ppGpp across the interface. Spheres represent Na^+ ions. Dashed lines represent hydrogen bonding measured in Å. **(c)** Overlay of ppGpp-bound XPRT (green) and GMP-bound XPRT (pink; PDB ID **2FXV**) shows that the 3'-phosphates are important for electrostatic interactions across the interface. ppGpp, GMP, Arg80, ppGpp's 3'-phosphates, and the bridging loop is labeled. Loop II is hidden for clarity. **(d)** Relative activity of XPRT at varied concentrations of GTP, GDP, and GMP. Error bars represent SEM of three replicates. **(e)** Size exclusion chromatograms of *B. subtilis* XPRT at 10 or 20 μM. ppGpp was added in the mobile phase. Vertical lines show the predicted retention volumes of monomeric and dimeric XPRTs based on their molecular

weight (see Materials and Methods). The higher absorbance with ppGpp is likely due to ppGpp absorbing at A_{280}.

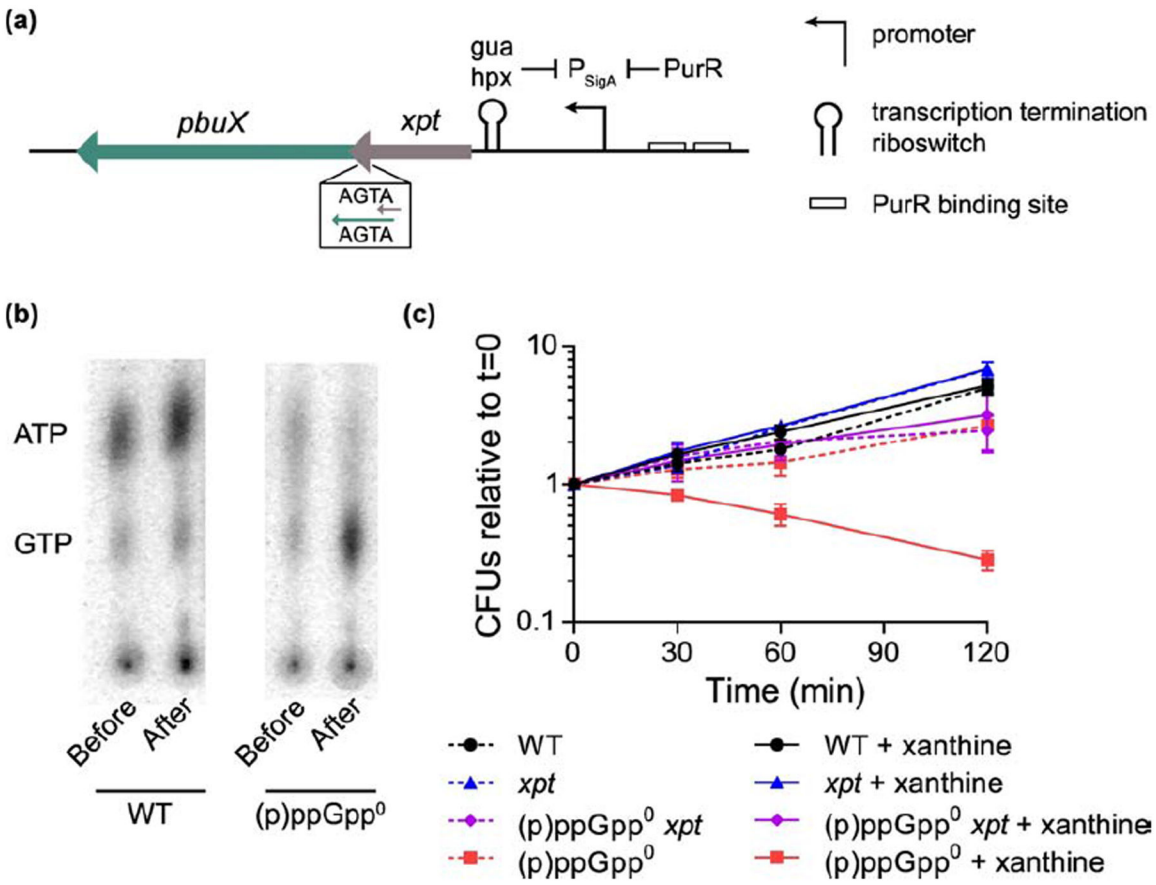

Figure 7. (p)ppGpp protects GTP homeostasis against excess environmental xanthine.

(a) Genomic locus of *xpt*, which encodes XPRT. The *xpt* gene is in the same operon as *pbuX*, which encodes the xanthine permease. Gene expression is controlled by the purine repressor PurR and a transcription attenuation riboswitch that binds hypoxanthine (hpx) and guanine (gua). **(b)** Thin layer chromatography showing GTP and ATP in ^{32}P-orthophosphate-labeled wild type and (p)ppGpp^0 *B. subtilis* before and after 30 min of treatment with 1 mM xanthine. Data are representative examples taken from the same TLC plate. **(c)** Viability of wild type, *xpt*::*kan*, (p)ppGpp^0, and (p)ppGpp^0 *xpt*::*kan B. subtilis* with and without 1 mM xanthine over a 120 min time course. Xanthine was added to logarithmically growing cultures, and colony forming units (CFUs) were determined for cultures with and without xanthine (solid and dashed lines, respectively). Error bars represent SEM of triplicate.

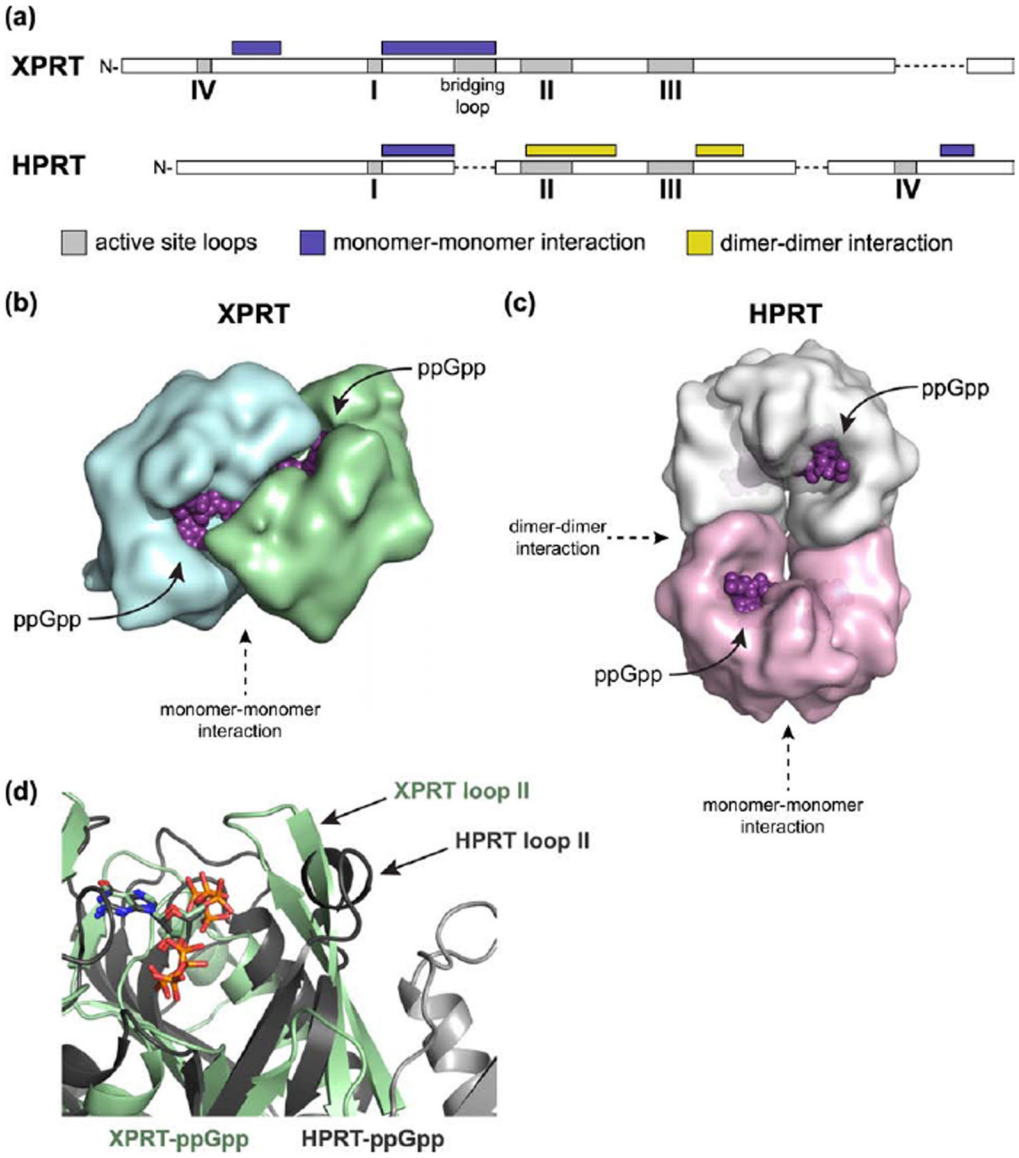

Figure 8. XPRT is allosterically regulated by ppGpp differently than HPRT due to distinct oligomeric interactions.

(a) Schematic of HPRT and XPRT architecture. Protein structures aligned with PROMALS3D. Gray boxes represent active site loops (I-IV). Regions marked with purple and yellow boxes are involved in monomer-monomer and dimer-dimer interactions, respectively. Dashed lines indicate a break in alignment. **(b)** Surface representation of an XPRT dimer bound to ppGpp. Note the intersubunit binding site that allows XPRT to cooperatively bind ppGpp. **(c)** Surface representation of an HPRT tetramer bound to ppGpp (PDB ID **6D9S**). The dimer-dimer interaction allosterically affects the conformation of the ppGpp binding pocket. **(d)** Overlay of XPRT-ppGpp (green) and HPRT-ppGpp (gray) showing the difference in the positioning of loop II. Loop II in HPRT forms a dimer-dimer interaction that holds it away from the binding pocket. Light gray cartoon represents an

additional HPRT subunit. The second monomer in the XPRT dimer is hidden to better show the (p)ppGpp binding pocket, which is otherwise obscured by the bridging loop.

Table 1.

Parameters of alarmone interaction with XPRT

	K_d (μM)	n_H	IC_{50} (μM)	n_{app}
pppGpp	9.6 ± 2.2	1.3 ± 0.2	56.4 ± 1.8	1.5 ± 0.1
ppGpp	0.95 ± 0.03	2.1 ± 0.1	3.3 ± 0.1	1.7 ± 0.1
pGpp	0.76 ± 0.04	2.3 ± 0.2	0.96 ± 0.04	1.6 ± 0.1

IC_{50} = half maximal inhibitory concentration

n_H = Hill coefficient from binding curve

n_{app} = apparent Hill coefficient from inhibition curve

± standard error

Table 2.

XPRT-ppGpp structure re-refinement statistics.

Refinement	
Resolution range (highest resolution bin) (Å)	34.23 – 1.8 (1.864 – 1.8)
R_{work}/R_{free} [a] (%)	15.98 / 20.83
r.m.s.[b] deviations	
Bonds (Å)	0.0038
Angles (Å)	0.76
Ramachandran statistics (%)	
Favored	96.21
Allowed	3.66
Disallowed	0.13
Rotamer outliers (%)	0.00
No. atoms	
Macromolecules	11763
Ligands	188
Solvent	756
B factor (Å^2)	
Macromolecules	25.98
Ligands	25.31
Solvent	33.25

[a] $R_{work}/R_{free} = \Sigma||F_{obs}|-|F_{calc}||/|F_{obs}|$, where the working the free R factors are calculated by using the working and free reflection sets, respectively. The free R reflections were held aside throughout refinement.

[b] Root mean square

Table 3.

List of primers, plasmids, and strains

Category	ID	Sequence (5' to 3') or Construct	Purpose	Source
Primer	oJW902	AAAGAGGCGCTTTTGACGTG	Verify *relA*::*cat* genotype	
Primer	oJW903	TTGTTGACCCGGGACATGGA	Verify *relA*::*cat* genotype	
Primer	oJW2298	ACTCAGTGGCACGAACTTGT	Amplify *xpt*::*kan*	
Primer	oJW2303	GCGGATGGAATAATAGTCGTGAAAG	Amplify *xpt*::*kan*	
Primer	oJW492	GCTTTGTTAGCAGCCGGATCAG	Amplify pLIC-trPC-HA insert	
Primer	oJW1124	CCGCACCTGTGGCGCCGGTG	Amplify pLIC-trPC-HA insert	
Primer	oJW1974	TACTTCCAATCCAATGCAATGGAAGCACTGAAACGGAA	Amplify *B. subtilis xpt* for LIC cloning	
Primer	oJW1975	TTATCCACTTCCAATGTTATTATGAATGAACCTCCTGTACGA	Amplify *B. subtilis xpt* for LIC cloning	
Primer	oJW3364	CTGTCCATTTGCCAATAAATCATCGATAATCAGCACATGATCCT	QuikChange mutagenesis for XPRT F126L	
Primer	oJW3365	AGGATCATGTGCTGATTATCGATGATTTATTGGCAAATGGACAG	QuikChange mutagenesis for XPRT F126L	
Primer	oJW3366	GCCTGTCCATTTGCCAAAATATCATCGATAATCAGCACA	QuikChange mutagenesis for XPRT F126I	
Primer	oJW3367	TGTGCTGATTATCGATGATATTTTGGCAAATGGACAGGC	QuikChange mutagenesis for XPRT F126I	
Primer	oJW3368	GCGCTGCCTGTCCAGCTGCCAAAAAATCATCGATAATCAGCA	QuikChange mutagenesis for XPRT N129A	
Primer	oJW3369	TGCTGATTATCGATGATTTTTTGGCAGCTGGACAGGCAGCGC	QuikChange mutagenesis for XPRT N129A	
Primer	oJW3372	TCCCGGCTGAAATGACTCTTCAATAACAATGCCGATTC	QuikChange mutagenesis for XPRT K156E	
Primer	oJW3373	GAATCGGCATTGTTATTGAAGAGTCATTTCAGCCGGGA	QuikChange mutagenesis for XPRT K156E	
Primer	oJW3926	GATTTATGCTTTGCCGCGAAGAC	Megaprimer mutagenesis for XPRT R80A	
Primer	oJW3927	GATTTATGCTTTTCCGCGAAGAC	Megaprimer mutagenesis for XPRT R80E	
Plasmid	pMCSG7	pLIC-trPC-HA	Expression vector	[43]
Plasmid	pJW536	pLIC-trPC-HA *B. subtilis xprT*	Expression of *B. subtilis* XPRT	This work
Plasmid	pJW725	pLIC-trPC-HA *B. subtilis xprT (F126I)*	Expression of *B. subtilis* XPRT F126L	This work

Category	ID	Sequence (5' to 3') or Construct	Purpose	Source
Plasmid	pJW726	pLIC-trPC-HA *B. subtilis xprT (F126L)*	Expression of *B. subtilis* XPRT F126I	This work
Plasmid	pJW727	pLIC-trPC-HA *B. subtilis xprT (N129A)*	Expression of *B. subtilis* XPRT N129A	This work
Plasmid	pJW728	pLIC-trPC-HA *B. subtilis xprT (K156E)*	Expression of *B. subtilis* XPRT K156E	This work
Plasmid	pJW729	pLIC-trPC-HA *B. subtilis xprT (R80A)*	Expression of *B. subtilis* XPRT R80A	This work
Plasmid	pJW730	pLIC-trPC-HA *B. subtilis xprT (R80E)*	Expression of *B. subtilis* XPRT R80E	This work
Strain		*E. coli* BL21(DE3)	Protein expression strain	NEB
Strain	JDW2144	*Bacillus subtilis* NCIB 3610 lacking pBS32	Wild type *B. subtilis*	[55]
Strain	JDW2231	*Bacillus subtilis* NCIB 3610 lacking pBS32 Δ*yjbM* Δ*ywaC relA*::*mls*	(p)ppGpp^0 *B. subtilis*	[56]
Strain	JDW4008	JDW2144 *xprT*::*kan*	Δ*xpt*	This work
Strain	JDW4022	*Bacillus subtilis* NCIB 3610 lacking pBS32 Δ*yjbM* Δ*ywaC relA*::*cat xprT*::*kan*	(p)ppGpp^0 Δ*xpt*	This work
Strain	CF5766	BL21(DE3)/pHM504 (pT7 GppA) Ap	Express GppA for ppGpp synthesis	[40]
Strain	CF7955	BL21(DE3)/pHM138 1 (pUM99) (pT7 Rel*Seq*1–385H) Ap	Express Rel*Seq* for (p)ppGpp synthesis	[40]